

An *Ab Initio* Study on Energy Gap of Bilayer Graphene Nanoribbons with Armchair Edges

Kai-Tak Lam^a and Gengchiao Liang^b

Department of Electrical and Computer Engineering, National University of Singapore

Dependency of energy bandgap (E_g) of bilayer armchair graphene nanoribbons (AGNR_B) on their widths, interlayer distance (D) and edge doping concentration of boron/nitrogen is investigated using local density approximation and compare to the results of monolayer graphene nanoribbons (AGNR_M). Although E_g of AGNR_B, in general, is smaller than that of AGNR_M, AGNR_B exhibits two distinct groups, metal and semiconductor, while AGNR_M displays purely semiconducting behavior. E_g of AGNR_B, moreover, is highly sensitive to D , indicating a possible application in tuning E_g by varying D . Finally, edge doping of both AGNR systems reduces E_g by 11-17%/4-10% for AGNR_M/AGNR_B, respectively.

^a lamkt@nus.edu.sg

^b elelg@nus.edu.sg

Carbon related materials recently have generated much interest due to their unique physical, electronic, and optical properties. Carbon atoms arranged in a linear honeycomb structure in a two dimension (2D) plane form graphene sheets which are the basis for many other carbon nanostructures such as fullerenes, carbon nanotubes and graphene nanoribbons. Recent experiments¹⁻³ show the possibility to cut or pattern the 2D graphene sheet into nanometer width strips named graphene nanoribbons (GNRs). GNRs have different electrical properties compared to graphene sheets due to quantum confinement as well as the abrupt terminations at the edges. From tight-binding⁴⁻⁶ and first-principles calculations⁷⁻¹⁰, these GNRs are semiconducting materials with an energy gap (E_g) dependent on the ribbon width as well as the atomic configuration of the edges. More specifically, for GNRs with armchair edges, the E_g decreases with increasing width, exhibiting 3 distinct trends in the E_g variations. Application of GNR in field-effect transistor devices has also been studied theoretically¹¹⁻¹⁵ and experimentally¹⁻³. In order to keep the high performance, doped source and drain in field effect transistors are required. GNRs provide the possibility to substitute the edge carbon atoms with either boron or nitrogen which will lead to a *p*-type or *n*-type doped semiconductor, respectively^{12,13,16}. Apart from monolayer GNRs, recent experimental¹⁷⁻¹⁹ and theoretical²⁰ studies are also carried out based on bilayer graphene and they show that bilayer graphene has unique features such as anomalous integer quantum Hall effects¹⁷ and the ability to control the size of E_g by adjusting carrier concentration¹⁸ as well as by an external electric field¹⁹. These unique properties open up the opportunity to implement bilayer GNRs in the various applications.

Understanding the stable geometry of bilayer GNRs, their electronic structures, and their fundamental physics is the essential steps towards device realization. In this

letter, therefore, we investigate the electronic structure of armchair-edge bilayer GNRs (AGNR_B) and the dopant effects on bandgap using first-principles calculations based on Density Functional Theory (DFT) within local density approximation, implementing the self-consistent pseudopotential method and the double- ζ (polarized) basis set by the conventional software package, Atomistix ToolKit 2.2²¹⁻²³. We first determine the optimum interlayer distance of AGNR_B based on the total energy calculations as function of the interlayer distance. We found that the optimum interlayer distance of AGNR_B is smaller than that of bilayer graphene due to non-uniform charge distribution in AGNR_B. Then, we examine the effect of interlayer distance on E_g of AGNR_B, followed by the width dependency of E_g of AGNR_B and contrast it with that of armchair-edge monolayer GNRs (AGNR_M). Like AGNR_M, AGNR_B also shows three different groups in terms of E_g dependence on width, and in general, AGNR_B is found to have a lower E_g than AGNR_M. Especially for $N=3p+2$ family, while it is semiconducting for AGNR_M⁸, the E_g of AGNR_B is very small and can be considered as metallic at room temperature. Furthermore, we investigate the relationship between E_g and the interlayer distance (D) of AGNR_B, and E_g is found to be strongly influenced by D . Finally, we present the edge doping effect on both AGNR_M and AGNR_B, which are found to form p -type and n -type semiconductor with boron and nitrogen.

Following the nomenclature in Ref. 8 and references within, the width of the AGNR_M is related to the number of dimer lines (N) across the ribbon width. The honeycomb structure, with hydrogen-passivation, of AGNR_M with $N=7$ (or 7-AGNR_M) is shown in Fig. 1(a). The carbon-carbon bond and the carbon-hydrogen bond are set at 1.42Å and 1.09Å, respectively and the structure is allowed to relax until the forces between the atoms are less than 0.05eV/Å. The boxed regions in Fig. 1(a) indicated

the sites where boron and nitrogen atoms are more energetically favorable to replace a carbon atom¹².

In a bilayer graphene, the two graphene sheets are arranged with the atoms in one layer located on top of the center of a hexagon in the other layer (shown in Fig. 1(b)). This arrangement is commonly found in nature²⁴ and previous calculation had shown that it is the most energetically favorable configuration²⁵. The total energy of an AGNR_B is calculated by stacking 2 AGNR_M in similar fashion in the simulation. The total energy of a structure where the AGNR_M are directly above each other is also calculated and the results show that the former structure has a lower total energy, indicating a more energetically favorable AGNR_B . Similar to the nomenclature of AGNR_M , a 7- AGNR_B is shown in Fig. 1(c).

In order to determine the optimum interlayer distance (D) between the GNR in an AGNR_B , the total energy of a 7- AGNR_B ²⁶ is calculated as D varies. For comparison, the total energy of a bilayer graphene²⁶ with varying D has also been calculated and the normalized results shown in Fig. 2(a). The results show that there are two stable energy points for both bilayer graphene and AGNR_B as D varies. For $D > 4.9 \text{ \AA}$, the total energy become a plateau as D varies, indicating the interaction between the layers is negligible at a distance larger than 4.9 \AA . For $D < 4.9 \text{ \AA}$, the interlayer interactions become significant and the total energy of the system quickly reaches a minimum at $D \approx 3.3 \text{ \AA}$ for bilayer graphene. It is in a good agreement with previous first-principles calculation²⁵ which showed that the interlayer distance for bilayer graphene was around 3.4 \AA . Using 7- AGNR_B as an example, we found that the minimum energy occurs at $D \approx 3.1 \text{ \AA}$. To investigate the variation on interlayer distance between infinite bilayer graphene and AGNR_B , the charge density in the plane between the layers for bilayer graphene and 7- AGNR_B are plotted in Fig. 2(b)

and (c) respectively. For bilayer graphenes, the charges are concentrated at the points where the carbon atoms of the two layers are aligned, and periodically distributed along the entire plane. Comparatively, the charges are not as strongly localized at the aligned carbon atoms for 7-AGNR_B, but there are more charge accumulation at the edges of 7-AGNR_B. Furthermore, we found that as AGNR_B width increase, the optimum D increases, as shown in the insert of Fig. 2(a). This suggested that edge-effect plays an important role in charge distributions and in determining the optimum D of an AGNR_B.

Next, the energy gap (E_g) dependency on the width (W) of AGNR_B is investigated, as shown in Fig. 3(a). We first examine the case where $D=6.5\text{\AA}$ (hollow points) where the interlayer interaction is not significant following the calculations above. The E_g of this system shows three families ($N=3p, 3p+1, 3p+2$, p is a positive integer) which exactly match the monolayer trends (dot-dashed lines). It indicates that an AGNR_B with large D can be treated as two AGNR_M in terms of electronic structure. On the other hand, at their respective optimum D (D_{op}) which is different at different width of AGNR_B, the E_g of AGNR_B (solid points in Fig. 3(a)) is smaller by 32-96% as compared to that of AGNR_M. More specifically, for the family of $N=3p+2$, the E_g of AGNR_B is very small (in the range of 15-30meV) and it can be considered as metallic materials at room temperature. However, for AGNR_M, this family exhibits a relatively large E_g and is considered as semiconductor materials, similar to the other two families. According to Ref. 8, E_g of this family is strongly affected by the edge effect of AGNR_M. However for AGNR_B, there exists an electron-electron interaction between the layers at the edges and hence the edge effect diminishes as compared to AGNR_M, which leads to the metallic nature for this family of AGNR_B. For $N=3p+1$, the E_g of AGNR_B is larger than the $N=3p$ family at small W . At larger W , the E_g of

$N=3p+1$ decreases dramatically and becomes similar to that of $N=3p$. It indicates that the edge exerts less effect on E_g when the AGNR_B width is over 2.4nm. In addition to the variation in W , the E_g of AGNR_B is also affected by the interlayer distance (D) and the E_g dependency on D for $N=5, 6$ and 7 is presented in Fig. 3(b). For D larger than the respective D_{op} , E_g increases as D increases, with $N=3p+1$ showing the largest increment. Conversely, as D decreases, E_g decreases. Therefore, it is indicated that the electronic properties of AGNR_B can be controlled by the width of the ribbon as well as the interlayer distance. This opens up another possible avenue for device design using bandgap engineering.

Finally, we explore the edge doping effects of AGNR_M and AGNR_B on their electronic structures. Edge doping concentration is defined as the number of dopant atoms, boron (triangle) and nitrogen (diamond), per unit length per layer of AGNR_M¹³. The most energetically favorable doping site is along the edges of the ribbons¹² and it is shown in the boxed regions of Fig. 1(a). In order to understand the change in Fermi level, $N=7$ is chosen for both AGNR_M (red) and AGNR_B (blue). As shown in Fig. 4, the Fermi level of both AGNR_M and AGNR_B decreases as the concentration of boron increases, which corresponds to the formation of a p -type semiconductor. Similarly, as the concentration of nitrogen increases, the Fermi level of both AGNR systems increases, showing an n -type semiconductor. This confirms that both AGNR_M and AGNR_B can form doped semiconductor with suitable atoms attached at the edges. Furthermore, the E_g values for the doped AGNR systems are calculated and it is found that the E_g of AGNR_M decreases by 11-17% while that of AGNR_B decreases by 4-10%. Therefore, AGNR_B exhibits more stable electronic property than AGNR_M.

In this Letter, we explore the fundamental energy bandgap of armchair-edge bilayer GNR (AGNR_B) based on the first-principles calculations. Our simulations

show that the optimum interlayer distance (D) is about 3.1\AA for 7-AGNR_B, which is different from the interlayer distance ($D\approx 3.3\text{\AA}$) of bilayer graphene due to the difference in charge distribution between the layers. We also examine the width dependency of the energy gap (E_g) of AGNR_B and compared with that of monolayer GNR (AGNR_M). The E_g of AGNR_B is generally smaller than AGNR_M and unlike AGNR_M, one group ($N=3p+2$) of the E_g trends shows metallic behavior. Furthermore, we investigated the effect of interlayer distance on E_g of AGNR_B and found that E_g strongly depends on D . It indicates possible application in devices where E_g can be tuned by varying D . The edge doping concentration in AGNR_M and AGNR_B is also investigated and it shows that the Fermi level is changed by the type and concentration of the dopant, forming p -type (with boron) and n -type (with nitrogen) semiconductor. The study on the electronic structure of AGNR_B is an important precursor to the study of future AGNR_B devices. Although the E_g of AGNR_B is smaller than that of AGNR_M, recent study¹⁸ has shown that an externally applied electric field can open up the E_g of a bilayer graphene and this may also be applicable to AGNR_B.

This work was supported by the Ministry of Education of Singapore under Grant Nos. R-263-000-416-112 and R-263-000-416-133, and National Research Foundation CRP grant.

Reference

1. X. Li, X. Wang, L. Zhang, S. Lee and H. Dai, *Science* **319** (5867), 1229-1232 (2008).
2. K.S. Novoselov, A.K. Geim, S.V. Morozov, D. Jiang, Y. Zhang, S.V. Dubonos, I.V. Grigorieva and A.A. Firsov, *Science* **306** (5696), 666-669 (2004).
3. C. Berger, Z. Song, X. Li, X. Wu, N. Brown, C. Naud, D. Mayou, T. Li, J. Hass, A.N. Marchenkov, E.H. Conrad, P.N. First, W.A. de Heer, *Science* **312** (5777), 1191 (2006).
4. M. Fujita, K. Wakabayashi, K. Nakada and K. Kusakabe, *J. Phys. Soc. Jpn.* **65** (7), 1920 (1996).
5. L. Brey, H.A. Fertig, *Phys. Rev. B* **73**, 235411 (2006).
6. K. Nakada and M. Fujita, G. Dresselhaus and M.S. Dresselhaus, *Phys. Rev. B* **54** (24), 17954 (1996).
7. M. Ezawa, *Phys. Rev. B* **73** (4), 045432 (2006).
8. Y.W. Son, M.L. Cohen and S.G. Louie, *Phys. Rev. Lett.* **97** (21), 216803 (2006).
9. L. Yang, C.-H. Park, Y.W. Son, M.L. Cohen and S.G. Louie, *Phys. Rev. Lett.* **99**, 186801 (2007).
10. Y.W. Son, M.L. Cohen and S.G. Louie, *Nature* **444** (7117), 347 (2006)
11. G. Liang, N. Neophytou, D.E. Nikonov and M.S. Lundstrom, *IEEE Transactions on Electron Devices* **54** (4), 677 (2007).
12. Q. Yan, B. Huang, J. Yu, F. Zheng, J. Zang, J. Wu, B.L. Gu, F. Liu and W. Duan, *Nano Lett.* **7** (6), 1469 (2007).
13. B. Huang, Q. Yan, G. Zhou, J. Wu, B.L. Gu, W. Duan and F. Liu, *Appl. Phys. Lett.* **91** (25), 253122 (2007).
14. G. Liang, N. Neophytou and M.S. Lundstrom, *J. Appl. Phys.* **102** (5), 054307 (2007)
15. Y. Ouyang, Y. Yoon and J. Guo, *IEEE Transactions on Electron Devices* **54** (9), 2223 (2007).
16. T.B. Martins, R.H. Miwa, J.R.d.S. Antonio and A. Fazzio, *Phys. Rev. Lett.* **98** (19), 196803 (2007).

17. K.S. Novoselov, E. McCann, S.V. Morozov, V.I. Fal'ko, M.I. Katsnelson, U. Zeitler, D. Jiang, F. Schedin and A.K. Geim, *Nat. Phys.* **2** (3), 177 (2006).
18. T. Ohta, A. Bostwick, T. Seyller, K. Horn and E. Rotenberg, *Science* **313** (5789), 951 (2006).
19. E.V. Castro, K.S. Novoselov, S.V. Morozov, N.M.R. Peres, J.M.B. Lopes dos Santos, J. Nilsson, F. Guinea, A.K. Geim and A.H. Castro Neto, *Phys. Rev. Lett.* **99** (21), 216802 (2007).
20. M.I. Katsnelson, K.S. Novoselov and A.K. Geim, *Nat. Phys.* **2** (9), 620 (2006).
21. M. Brandbyge, J.L. Mozos, P. Ordejón, J. Taylor, and K. Stokbro, *Phys. Rev. B* **65** (16), 165401 (2002).
22. J.M. Soler, E. Artacho, J.D. Gale, A. Garcia, J. Junquera, P. Ordejón, and D. Sánchez-Portal, *Journal of Physics: Condensed Matter* (11), 2745 (2002).
23. J. Taylor, H. Guo, and J. Eang, *Phys. Rev. B* **63** (24), 245407 (2001).
24. A.H.C. Neto, F. Guinea, N.M.R. Peres, K.S. Novoselov and A.K. Geim, [arXiv.org:0709.1163] (2007).
25. S.B. Trickey, F. Muller-Plathe, G.H.F. Diercksen and J.C. Boettger, *Phys. Rev. B* **45** (8), 4460 (1992).
26. The super cell of a bilayer graphene consists of a total of 8 carbon atoms (4 per layer) while that of the 7-AGNR_B consists of 28 carbon atoms (14 per layer). A padding of 5Å is reserved for the top and bottom of the super cells. In addition, same padding is added at the armchair edges of 7-AGNR_B and 8 hydrogen atoms are included to passivate those edges.

Figure Captions

Fig. 1 (a) The honeycomb structure of a 7-AGNR_M. (b) The stacking configuration of a graphene bilayer. The top carbon layer (gold) is arranged such that one atom is positioned in the centre of the hexagon of the bottom layer (blue). (c) The atomic structure of a 7-AGNR_B with D representing the interlayer distance.

Fig. 2 (a) Total energy of a bilayer graphene and 7-AGNR_B as a function of the interlayer distance (D). Total energy is normalized as a ratio to the lowest value of the respective structure in the data. The optimum D (at lowest energy) of a bilayer graphene and 7-AGNR_B are 3.3Å and 3.1Å, respectively. Moreover, as $D > 4.9Å$, total energy in both cases shows saturation and it indicates that bilayer graphene sheets and GNR_B may behave like the monlayer graphene sheets and GNR_M. Insert shows that the optimum D increases as width of the AGNR_B increases. (b) and (c) show the charge density of the planes in the middle of the bilayer graphene and 7-AGNR_B, respectively. The unit of the color gradient bar is $1/\text{Bohr}^3$. The difference in charge distribution in these two cases causes the deviation in optimum D in Fig. 2(a).

Fig. 3 (a) Energy gap (E_g) as a function of the width of AGNR_B for interlayer distance (D)=6.5Å (hollow points) and the respective optimum D (solid points). Diamond, circle, and square points represent the three different families of $N=3p$, $3p+1$ and $3p+2$, respectively. Unlike AGNR_M, the family of $N=3p+2$ in AGNR_B shows almost zero bandgap for any width. The dot-dash lines show the three trends in AGNR_M which coincide with the E_g trends of AGNR_B when $D=6.5Å$. It demonstrates that AGNR_B with $D=6.5Å$ shows the same behaviors as AGNR_M. (b) Dependence of E_g

on D of the $AGNR_B$ for $N=5, 6$ and 7 . Electronic structure of $AGNR_B$ strongly depends on its interlayer distance.

Fig. 4 Fermi level *vis-a-vis* different boron (triangle) and nitrogen (diamond) doping concentrations for $7-AGNR_M$ (blue) and $7-AGNR_B$ (red). The dot-dash and dotted lines are the original Fermi level of undoped $7-AGNR_M$ and $7-AGNR_B$ respectively. It can be clearly seen that p -type (with boron) and n -type (nitrogen) semiconductors are formed with increasing dopant concentration. As doping concentration increases, bandgap of all four cases also decreases.

Figure 1, Lam, K.T. and Liang, G.C.

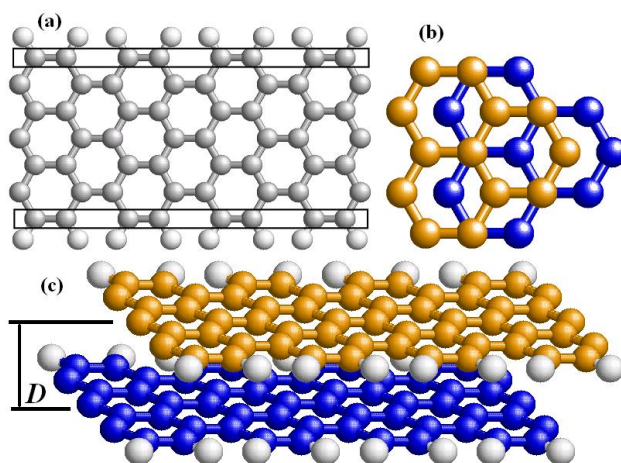


Figure 2, Lam, K.T. and Liang, G.C.

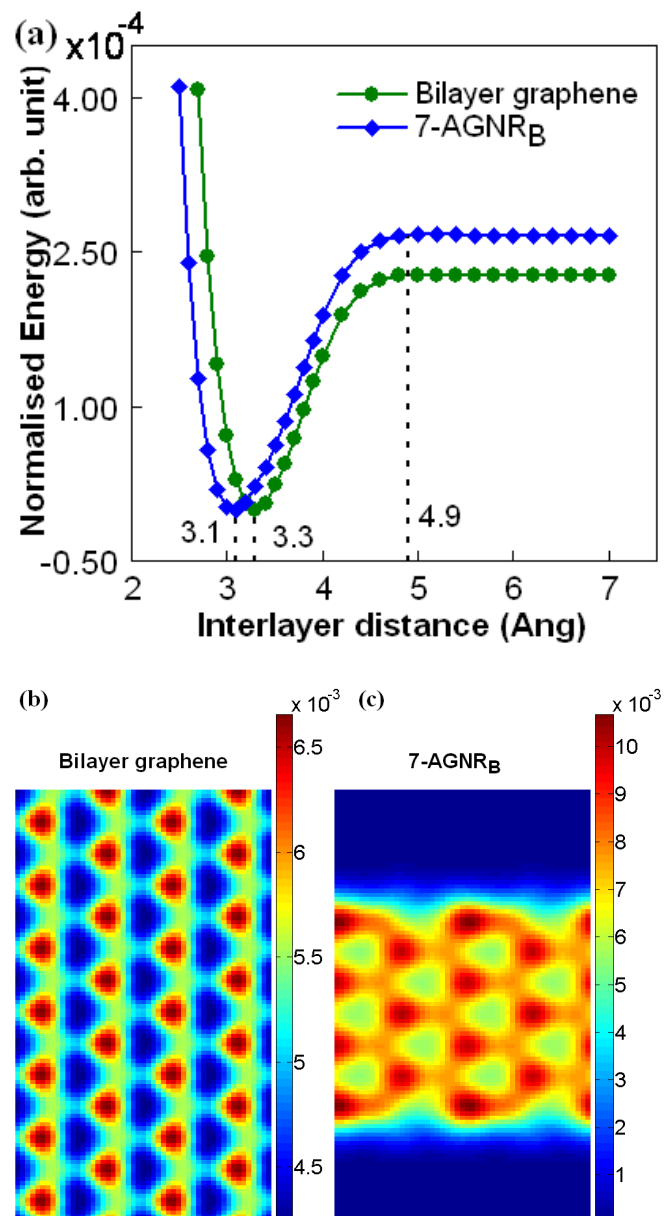


Figure 3, Lam, K.T. and Liang, G.C.

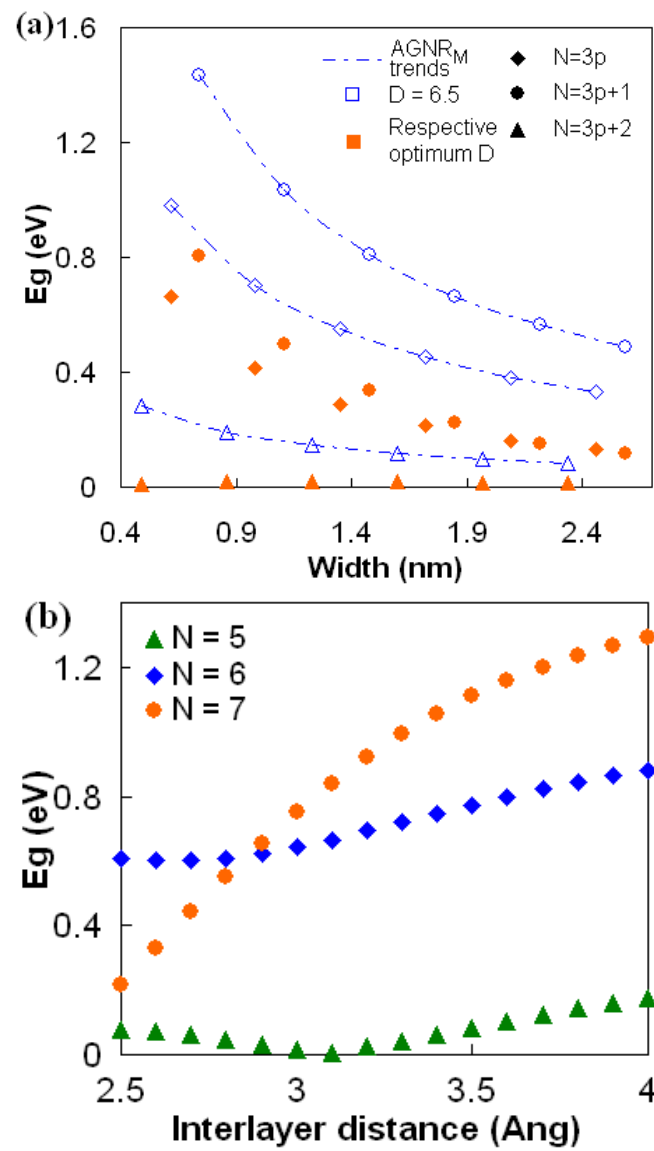


Figure 4, Lam, K.T. and Liang, G.C.

